Original Article

Evaluation of Kinetic and Equilibrium Parameters of $NiFe_2O_4$ Nanoparticles on Adsorption of Reactive Orange Dye from Water

Raziyeh Zandipak[*1], *Soheil Sobhanardakani*[2]

Received: 30.08.2015 *Accepted: 03.10.2015*

ABSTRACT

Background: Among different pollutants released into the environment, dyes are considered as one of the most dangerous contaminants. In recent years, magnetic nanomaterials have attracted much attention for their dye removal capacity. The aim of this study was to explore the adsorption kinetics of an anionic dye (Reactive Orange 13 (RO)) by $NiFe_2O_4$ nanoparticles ($NiFe_2O_4$ NPs) under various conditions.

Methods: $NiFe_2O_4$ nanoparticles ($NiFe_2O_4$ NPs) were prepared and characterized by X-ray diffraction (XRD), transmission electronic microscopy (TEM), pH_{pzc} and BET methods. The adsorption characteristics of the $NiFe_2O_4$ NPs adsorbent were examined using Reactive Orange 13 as an adsorbate. The influences of parameters including pH, dose of adsorbent and contact time were investigated to find the optimum adsorption conditions.

Results: Decreasing solution pH and increasing contact time were favorable for improving adsorption efficiency. The kinetic and isotherm data of RO adsorption on $NiFe_2O_4$ NPs were well fitted by pseudo-second-order and Langmuir models, respectively.

Conclusion: The maximal adsorption capacity of RO was 243.9 mg g^{-1} at 25°C and pH 3.0 and the adsorption of RO on the $NiFe_2O_4$ NPs follows a monolayer coverage model. $NiFe_2O_4$ NPs might be an effective and potential adsorbent for removing anionic dyes from aqueous solutions.

Keywords: Chemical Water Pollution, Coloring Agents, Magnetite Nanoparticles, Reactive Orange.

IJT 2016 (2): 51-58

INTRODUCTION

Synthetic dyes are commonly used in a number of industries, including textile, food, pharmaceutical, leather, cosmetic and paper plants, and their removal has been a difficult problem [1]. Their complex molecular structures make them very stable and difficult for biodegradation [2]. The discharge of dyes into the environment is a matter of concern as for their toxicological and carcinogenic hazards for human beings and esthetical influences on the environment [3, 4].

The presence of dyes in aqueous effluents poses serious ecological threats. These dyes cause reduction in photosynthetic action of aquatic vegetations and reduce light penetration into the water [5-7]. There are many procedures for the treatment of dye-containing wastewaters, such as biological treatment, coagulation/flocculation, chemical oxidation, membrane filtration, ion-exchange, photocatalytic degradation, and adsorption methods [8-11]. The most common technique is adsorption technology, which is popular for its effectiveness, efficiency, economy and absence of secondary pollution [12]. In recent years, magnetic nanomaterials have attracted much attention, since they not only have large removal capacity, fast kinetics and reactivity for contaminant removal, but also have high separation efficiency and reusability. Magnetic nanoparticles (NPs) with the general formula MFe_2O_4 (M = Fe, Co, Cu, Mn, Ni, etc.) have

1. MSc of Environmental Sciences, Young Researchers & Elite Club, Hamedan Branch, Islamic Azad University, Hamedan, Iran.

2. Department of the Environment, College of Basic Sciences, Hamedan Branch, Islamic Azad University, Hamedan, Iran.

*Corresponding Author: E-mail: r_zandi@iauh.ac.ir

become one of the most popular materials in terms of analytical biochemistry, medicine, removal of heavy metals and biotechnology, and have been increasingly applied to immobilize proteins, enzymes, and other bioactive agents due to their unique properties [13].

$NiFe_2O_4$ nanoparticles ($NiFe_2O_4$ NPs) are well-known adsorbents with good biocompatibility, strong super paramagnetic property, low toxicity, easy preparation and high adsorption ability [14]. $NiFe_2O_4$ NPs has an inverse spinel structure and shows ferrimagnetism that originates from magnetic moment of anti-parallel spins between Fe^{3+} ions at tetrahedral sites and Ni^{2+} ions at octahedral sites. $NiFe_2O_4$ NPs have high surface area and low mass transfer resistance. Moreover, the magnetic behavior of these nanoparticles depends mostly on their size [15].

The objective of this study was to investigate kinetics and isotherms of reactive orange dye (RO) removal by $NiFe_2O_4$ NPs. The effects of pH, adsorbent dose and contact time on the adsorption of RO were evaluated.

MATERIALS AND METHODS

Apparatus and Reagents

The concentration of dye in the solutions was measured using UV–Vis spectrophotometer (Lambda 45, Perkin Elmer, Waltham, USA). All pH measurements were executed with a 780 pH meter (Metrohm, Switzerland) using a glace-calomel electrode.

The crystal structure of synthesized materials was determined by XRD (38066 Riva, d/G.Via M. Misone, 11/D (TN) Italy) at ambient temperature. The structure of the $NiFe_2O_4$ NPs was characterized by transmission electronic microscopy (TEM, Philips, CM10, 100 KV). Specific surface area and porosity were evaluated by N_2 adsorption–desorption porosimetry (77 K) using porosimeter (Bel Japan, Inc.). The elemental analysis was measured by scanning electron microscope energy dispersive X-ray spectroscopy (SEM-EDX, XL 30 and Philips Netherland).

All chemicals and reagents used in this study were of analytical grade and were purchased from Merck Company (Merck, Darmstadt, Germany). Reactive orange dye (Fig. 1) was obtained from Alvan Sabet Company (Alvan Sabet Co. Iran). Stock solution of dye (10^{-3} M) was prepared by dissolving the appropriate amount of powder in double-distilled water. Double-distilled water (DDW) was used for preparation of all solutions.

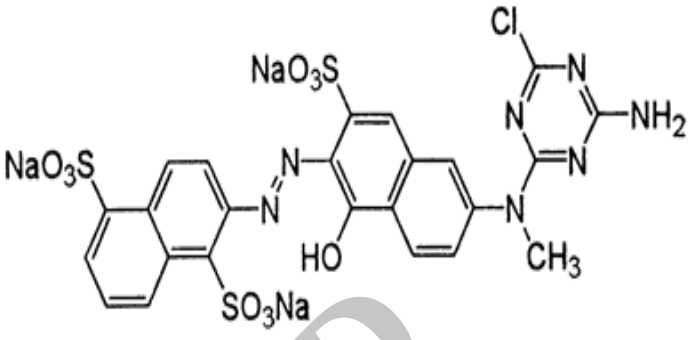

Figure 1. The chemical structure of Reactive Orange 13 (RO).

Synthesis of Nife$_2$o$_4$ Nps

The $NiFe_2O_4$ samples were prepared by co-precipitation method. In a typical synthesis, 0.2 M (20 mL) solution of iron nitrate [$(Fe(NO_3)_3.9H_2O)$] and 0.1 M (20 mL) solution of nickel nitrate [$(Ni(NO_3)_2.6H_2O)$] were prepared and vigorously stirred for 1 h at 80 °C. Additionally, 0.2 g of polyethylene oxide (PEO) was added to the solution as a capping agent. Subsequently, 5 ml of hydrazine hydrate ($NH_2.NH_2.H_2O$) was added drop by drop into the solutions and brown color precipitates were formed. Finally, the precipitates were separated by centrifugation and were dried in hot air oven for 4 h at 100 °C. The acquired substance was annealed for 10 h at 300 °C [16].

Point of Zero Charge Ph

The point of zero charge pH (pH_{pzc}) for the adsorbent was determined by introducing 0.03 g of $NiFe_2O_4$ NPs into eight 100 mL Erlenmeyer flasks containing 0.1 M $NaNO_3$ solution. The pH values of the solutions were adjusted to 2, 3, 4, 5, 6, 7, 8, 9 using solutions of 0.01 mol L^{-1} HNO_3 and NaOH. The solution mixtures were allowed to equilibrate in an isothermal shaker (25 °C) for 24 h. The final pH was measured after 24 h. The pH_{pzc} is the point where the $pH_{initial} = pH_{final}$.

Equilibrium and Kinetic Experiment

In each experiment, 15 mL dye solution (50 mg L^{-1}) was transferred into a 25 mL

stoppered conical flask. Then a weighed amount of adsorbent (0.03 g) was added to the solution and the pH of the solution was adjusted to 1–9, using 0.1 mol L^{-1} HCl and/or 0.1 mol L^{-1} NaOH solutions. The flask was then agitated at a constant speed (150 rpm) and in a temperature controlled shaking water bath. The samples were withdrawn at different time intervals and the adsorbent was separated by an external magnet and the concentrations of the dye that remained in the solution were determined by UV–visible spectrophotometry (Lambda 45, Perkin-Elmer, Waltham, USA) at 489 nm. The concentration of the remaining dye in the adsorbent phase (q_e, mg g^{-1}) were calculated using Eq. (1):

$$q_e = \frac{(C_0 - C_e)V}{W} \quad (1)$$

Where, C_0 and C_e (mg L^{-1}) are initial and equilibrium concentrations, respectively, V (L) is the volume of solution and W (g) is the mass of adsorbent [17, 18].

Finally, the RO removal efficiency was calculated using Eq. (2):

$$R\,(\%) = \frac{C_0 - C_e}{C_0} \times 100 \quad (2)$$

RESULTS

The X-ray diffraction pattern of $NiFe_2O_4$ NPs is shown in Fig. 2. The TEM micrograph and calculated histogram of the $NiFe_2O_4$ are illustrated in Fig. 3. In addition, Fig. 4 shows a typical SEM-EDX elemental analysis of $NiFe_2O_4$ NPs.

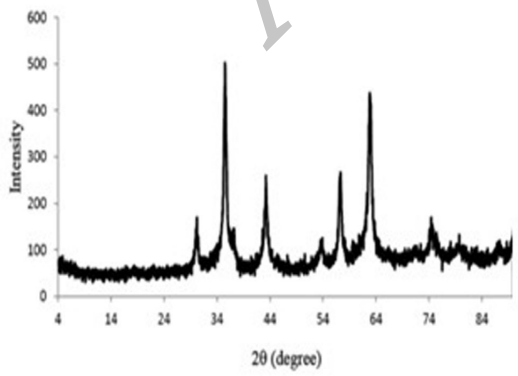

Figure 2. The X-ray diffraction pattern of $NiFe_2O_4$ NPs.

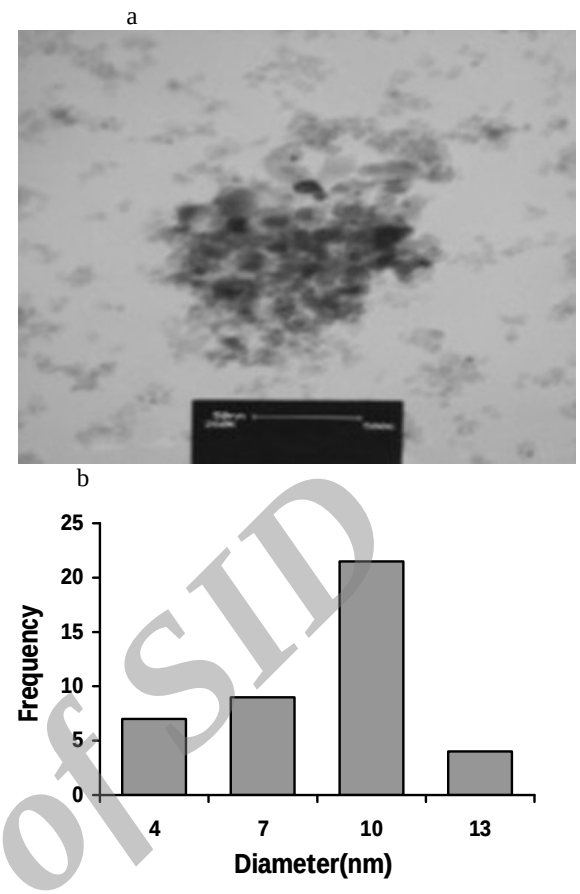

Figure 3. (a) TEM micrograph and (b) calculated histogram of $NiFe_2O_4$ NPs.

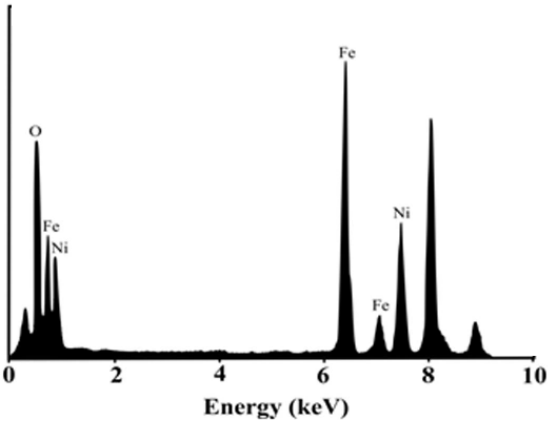

Figure 4. SEM-EDX spectrum of $NiFe_2O_4$ NPs.

The effects of initial pH on the percentage of removal of RO dye using $NiFe_2O_4$ adsorbent were evaluated within a pH range of 2.0 to 9.0 (Fig. 5b). The percentage of dye removal decreased when pH increased from 2.0 to 9.0. The highest RO removal ratio (95%) was achieved at pH 3.0. The point of zero charge (pH_{pzc}) value determined for $NiFe_2O_4$ adsorbent was 7.0 (Fig. 5a).

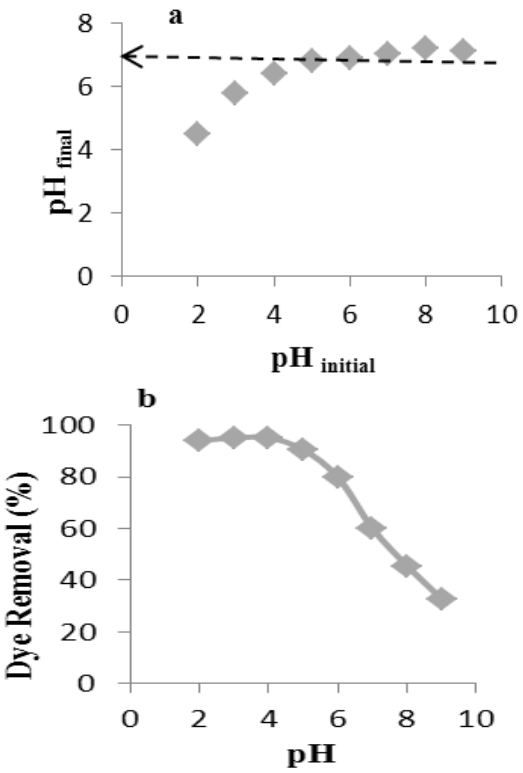

Figure 5. (a) Determination of the point of zero charge of $NiFe_2O_4$ NPs. (b) The effect of solution pH on the removal percentage of Reactive Orange dye by $NiFe_2O_4$ NPs.

The study of adsorbent dose for the removal of RO dye from aqueous solution was carried out using adsorbent doses ranging from 0.007 to 0.06 g of $NiFe_2O_4$ NPs, with fixing the initial dye concentration at 50 mg L^{-1}. The highest amount of dye removal was attained with an adsorbent dose of 0.03 g (Fig. 6).

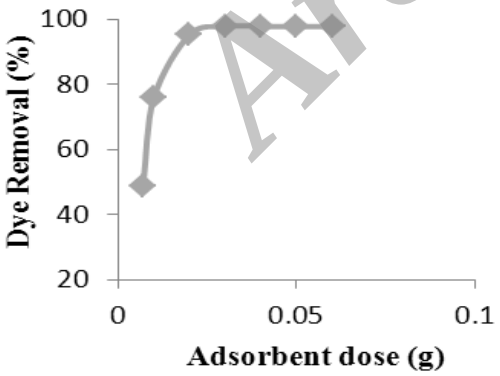

Figure 6. Effect of dose of $NiFe_2O_4$ NPs on the removal percentage of Reactive Orange dye.

The effect of contact time was evaluated to determine the time taken by $NiFe_2O_4$ NPs to remove 50, 100 and 150 mg L^{-1} dye solutions at optimum pH (Fig. 7).

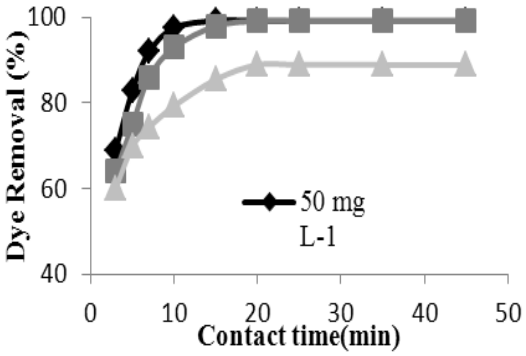

Figure 7. The effect of contact time on the removal percentage of Reactive Orange by $NiFe_2O_4$ NPs.

The experimental kinetic data of adsorption of RO dye onto $NiFe_2O_4$ NPs were examined using the pseudo-first-order and pseudo-second-order equations. The kinetic constants obtained by linear regression for the two models (Fig. 8) are summarized in Table 1.

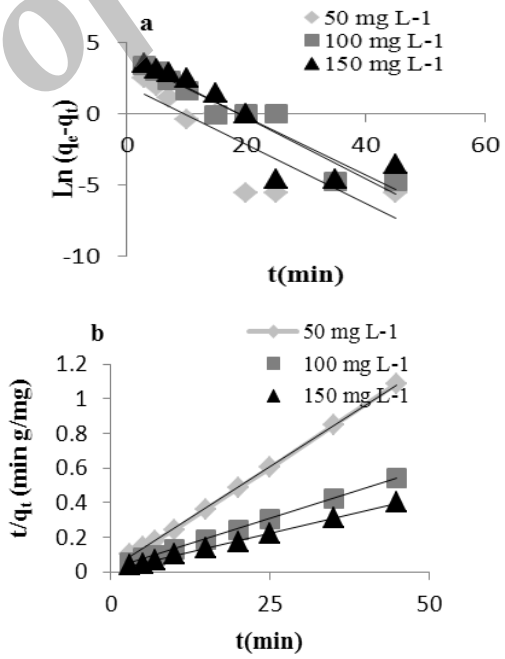

Figure 8. (a) Pseudo-first-order kinetic plot and (b) pseudo-second-order kinetic plot for the adsorption of Reactive Orange dye onto $NiFe_2O_4$ NPs at 25°C.

Adsorption isotherms of RO dye onto the $NiFe_2O_4$ NPs were obtained at pH 3.0 with various initial dye concentrations (50-450 mg L^{-1}) (Fig. 9). The adsorption constants obtained from the isotherms are listed in Table 2.

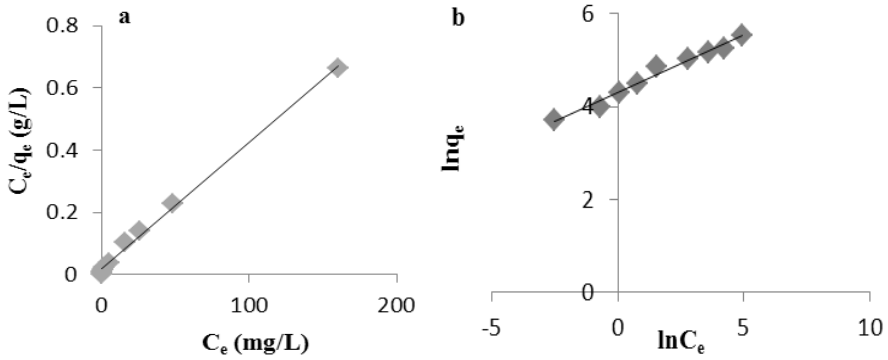

Figure 9. (a) Langmuir and (b) Freundlich isotherms for Reactive Orange dye adsorption onto $NiFe_2O_4$ NPs at 25 °C.

Table 1. Pseudo-first-order and pseudo-second-order kinetic model parameters for the adsorption of Reactive Orange dye onto $NiFe_2O_4$ NPs at 25°C.

	Pseudo-first-order kinetic model				Pseudo-second-order kinetic model		
C_0 (mg L^{-1})	q_e exp(mg g^{-1})	q_{e1}(mg g^{-1})	k_1 (min^{-1})	R^2	q_{e2} (mg g^{-1})	k_2 (g mg^{-1} min^{-1})	R^2
50	41.35	7.62	0.208	0.747	42.37	0.030	0.999
100	82.62	45.83	0.202	0.934	86.20	0.008	0.999
150	111.19	56.71	0.214	0.814	116.27	0.007	0.998

Table 2. Isotherm parameters of adsorption of Reactive Orange onto $NiFe_2O_4$ NPs at 25 °C.

Langmuir			Freundlich		
b (L mg^{-1})	q_m (mg g^{-1})	R^2	K_f ($mg^{1-(1/n)}$ $L^{1/n}$ g^{-1})	n	R^2
0.22	55 243.9	0.996	73.55	4.04	0.978

DISCUSSION

Fig. 2 shows the X-ray diffraction (XRD) patterns of $NiFe_2O_4$ NPs, where all the diffraction peaks of $NiFe_2O_4$ c are assigned to spinel type $NiFe_2O_4$ (JCPDS 54-0964). The peaks at the 2Θ values of 30.1, 35.3, 43.0, 53.7, 56.5, and 62.4° can be indexed to (111), (220), (311), (400), (422), (511) and (440) crystal planes of spinel $NiFe_2O_4$, respectively. The average crystallite size (D in nm) of $NiFe_2O_4$ NPs was determined from XRD pattern according to the Scherrer equation.

$$D = \frac{K\lambda}{\beta \cos\theta} \quad (3)$$

Where, λ is the wavelength of the X-ray radiation (1.5406 Å), K is a constant taken as 0.89, θ is the diffraction angle and β is the full width at half maximum (FWHM). The average size of $NiFe_2O_4$ NPs was calculated as around 15 nm. The TEM micrograph and calculated histogram of the $NiFe_2O_4$, (Fig. 3), reveals that the diameter of the synthesized $NiFe_2O_4$ NPs was around 12 nm. The particle size measured directly from the TEM micrograph agreed with that of the XRD results. Only Ni, Fe and O appeared in $NiFe_2O_4$ NPs samples (Fig. 4). Our results were in agreement with previous [14, 16].

Specific surface area is commonly reported as BET surface, obtained by applying the theory of Brunauer, Emmett, and Teller (BET) to nitrogen adsorption/desorption isotherms measured at 77 K. This is a standard procedure for determination of specific surface area of samples. The specific surface area of a sample is determined by physical adsorption of a gas on the surface of the solid and by measuring the amount of adsorbed gas corresponding to a monomolecular layer on the surface. Our data were treated according to BET's theory [19]. The results of BET method showed that the average specific surface area of $NiFe_2O_4$ NPs was 63.7 m^2 g^{-1}. The synthesized nanoparticles had relatively large specific surface areas and might be better for adsorption.

The pH of the solution in the adsorption process of dye molecules can affect both

aqueous chemistry and surface binding-sites of the adsorbent. In this study, the relationship between the initial solution pH and the adsorption efficiency was examined (Fig. 5b). RO dye adsorption decreased as the solution pH increased from 3.0 to 9.0. The effect of solution pH could be explained by the surface charge of the adsorbent. pH_{pzc} is an important property that indicates the electrical neutrality of the surface of the adsorbent at a particular value of pH. The pH_{pzc} for $NiFe_2O_4$ NPs was 7.0 [Fig. 5(a)]. At solution pHs higher than pH_{pzc}, the surface of the adsorbent has negative charge. Therefore, by increasing pH, the removal efficiency decreases because of decreased attractive forces between the anionic dye and negative surface charge. A similar behavior has been reported for RO adsorption on iron oxide nanospheres [20].

The adsorbent dose is an important parameter in adsorption studies, since it determines the capacity of adsorbent for a given initial concentration of dye solution. Fig. 6 presents the effect of $NiFe_2O_4$ NPs dose on the adsorption of RO dye. The adsorption efficiencies increased by increasing adsorbent dose. By increasing the $NiFe_2O_4$ NPs dose from 0.007 to 0.03 g, the removal efficiency (percent) of dye increased from 48.8% to 97.8%. The greater number of adsorption sites made available at higher NiFe2O4 NPs doses can explain this observation. Similar results were observed by Silva et al., who investigated the effect of dose of adsorbent on removal of dyes from aqueous solution by modified-KSF-montmorillonite, and indicated that adsorption efficiency increased with increasing adsorbent dose [21].

Equilibrium time is the major parameter in designing economic systems used for the treatment of wastewaters. We studied the effects of contact time on the adsorption. The removal efficiency increased rapidly at the beginning and then followed a slow increase, until the attainment of equilibrium stage. The reason might be the access of high number of vacant binding active sites for dye anions at the beginning and gradual covering of these binding sites, which decreased the adsorption speed and at the end when equilibrium was attained. Optimum contact times for $NiFe_2O_4$ NPs adsorbent were 15, 20 and 20 min, respectively, for 50, 100 and 150 mg L^{-1} initial dye concentration. Similar results have been found by Zhang et al. [22].

The kinetic data were analyzed using two commonly kinetic models, namely, the pseudo-first-order and the pseudo-second-order, which can be expressed in the linear forms as follows [23]:

$$\ln(q_e - q_t) = \ln(q_e) - \frac{k_1 t}{2.303} \quad (4)$$

$$\frac{t}{q_t} = \frac{1}{k_2 q_e^2} + \frac{t}{q_e} \quad (5)$$

Where, q_e and q_t are the amount of dye adsorbed (mg g^{-1}) at equilibrium and time t (min); k_1 is the rate constant of pseudo-first-order (min^{-1}); k_2 is the rate constant of pseudo-second-order (g mg^{-1} min^{-1}) for adsorption. The adsorption kinetic plots are shown in Fig. 8 and the related parameters calculated from the two models are listed in Table 1. The calculated determination coefficients (R^2) from the three initial dye concentrations of the pseudo-second-order kinetic model were higher than those of the pseudo-first-order kinetic model. This indicated that the pseudo-second-order model fitted the experimental data better. It could be used to describe the adsorption kinetics. The adsorption process fitted the pseudo-second-order model, which indicated that the rate-limiting step might be a chemical adsorption involving valence forces through sharing or exchanging of electrons between adsorbent and adsorbate.

The equilibrium adsorption isotherms are one of the most important figures that help to understand the mechanism of adsorption and describe how adsorbates could interact with adsorbents. In this study, the data collected have been fitted to the Langmuir and the Freundlich isotherms [24, 25], as described in Eqs. (6) and (7), respectively.

$$\frac{C_e}{q_e} = \frac{C_e}{q_m} + \frac{1}{q_m b_l} \quad (6)$$

$$\ln q_e = \frac{1}{n}\ln C_e + \ln k_f \quad (7)$$

Where, C_e (mg L^{-1}) is the equilibrium concentration of RO dye in solution, q_e (mg g^{-1}) is the equilibrium adsorption capacity of $NiFe_2O_4$ NPs, q_m (mg g^{-1}) is the maximum adsorption capacity of $NiFe_2O_4$ NPs for

monolayer coverage, b (L mg^{-1}) is a constant related to the adsorption free energy, K_f ($mg^{1-(1/n)}$ $L^{1/n}$ g^{-1}) is a constant related to adsorption capacity, and n is an empirical parameter related to adsorption. The linear fittings for two isotherm models are shown in Fig. 9.

The parameters predicted by the two different models are summarized in Table 2. From the values of the correlation coefficient (R^2) in Table 2, it is clear that the adsorption curves fitted better with the Langmuir isotherm than Freundlich isotherm, indicating that the adsorption of RO on the $NiFe_2O_4$ NPs adsorbent follows a monolayer coverage model. The maximum adsorption capacity (q_m) of RO on the $NiFe_2O_4$ NPs was calculated as 243.9 mg g^{-1}.

CONCLUSION

$NiFe_2O_4$ NPs were successfully synthesized by co-precipitation method and was used as an effective adsorbent for dye removal. According to TEM, the size of the nanostructures was calculated as around 12 nm. The amount of RO adsorbed on the $NiFe_2O_4$ NPs increased with increasing amounts of adsorbent and decreased with increases in pH. The Langmuir isotherm model fitted better Freundlich model. The maximal adsorption capacity of RO was 243.9 mg g^{-1} at 25˚C and pH 3.0. Kinetics results indicated that the RO adsorption followed the pseudo-second-order kinetic model.

ACKNOWLEDGEMENTS

The authors are grateful to Hamedan Branch, Islamic Azad University for providing facilities to conduct and complete this study. The authors declare that there is no conflict of interests.

REFERENCES

1. Zhang YR, Shen SL, Wang SQ, Huang J, Su P, Wang QR, Zhao BX. A dual function magnetic nanomaterial modified with lysine for removal of organic dyes from water solution. Chem Eng J 2014; 239:250–6.
2. Liu S, Ding Y, Li P, Diao K, Tan X, Lei F, Zhan Y, Li Q, Huang B, Huang Z. Adsorption of the anionic dye Congo red from aqueous solution onto natural zeolites modified with N,N-dimethyl dehydroabietylamine oxide. Chem Eng J 2014; 248:135–44.
3. Zhang W, Yang H, Dong L, Yan H, Li H, Jiang Z, Kan X, Li A, Cheng R. Efficient removal of both cationic and anionic dyes from aqueous solutions using a novel amphoteric straw-based adsorbent. Carbohydr Polym 2012; 90:887–93.
4. Ahmad MA, Alrozi R. Removal of malachite green dye from aqueous solution using rambutan peel-based activated carbon: Equilibrium, kinetic and thermodynamic studies. Chem Eng J 2011; 171: 510–6.
5. Sobhanardakani S, Zandipak R, Sahraei R. Removal of Janus Green dye from aqueous solutions using oxidized multi-walled carbon nanotubes. Toxicol Environ Chem 2013;95 (6): 909-18.
6. Zhu HY, Jiang R, Xiao L, Li W. A novel magnetically separable γ-Fe_2O_3/cross linked chitosan adsorbent: Preparation, characterization and adsorption application for removal of Hazardous azo dye. J Hazard Mater 2010; 179:251–7.
7. Cheung WH, Szeto YS, McKay G. Enhancing the adsorption capacities of acid dyes by chitosan nano particles. Bioresour Technol 2009; 100:1143–8.
8. Yao Y, Xu F, Chen M, Xu Z, Zhu Z. Adsorption behavior of methylene blue on carbon nanotubes. Bioresour Technol 2010; 101:3040–6.
9. Galán J, Rodríguez A, Gómez JM, Allen SJ, Walker GM. Reactive dye adsorption onto a novel mesoporous carbon. Chem Eng J 2013; 219:62–8.
10. Li DP, Zhang YR, Zhao XX, Zhao BX. Magnetic nanoparticles coated by aminoguanidine for selective adsorption of acid dyes from aqueous solution. Chem Eng J 2013; 232:425–33.
11. Janus M, Kusiak E, Choina J, Ziebro J, Morawski AW. Enhanced adsorption of two azo dyes produced by carbon modification of TiO_2. Desalination 2009; 249:359–63.
12. Ai L, Jiang J. Removal of methylene blue from aqueous solution with self-assembled cylindrical graphene–carbon nanotube hybrid. Chem Eng J 2012; 192:156–63.
13. Teymourian H, Salimi A, Khezrian S. Fe_3O_4 magnetic nanoparticles/reduced graphene oxide nanosheets as a novel electrochemical and bioeletrochemical sensing platform. Biosens Bioelectron 2013; 49:1–8.
14. Khosravi I, Eftekhar M. Characterization and evaluation catalytic efficiency of $NiFe_2O_4$ nanospinel in removal of reactive dye from aqueous solution. Powder Technol 2013; 250:147–53.
15. Patil JY, Nadargi DY, Gurav JL, Mulla IS, Suryavanshi SS. Synthesis of glycinecombusted

$NiFe_2O_4$ spinel ferrite: A highly versatile gas sensor. Mater Lett 2014; 124:144–7.
16. Sivakumar P, Ramesh R, Ramanand A, Ponnusamy S, Muthamizhchelvan C. Synthesis and characterization of $NiFe_2O_4$ nanoparticles and nanorods. J Alloys Compd 2013; 563:6–11.
17. Wang XS, Zhu L, Lu HJ. Surface chemical properties and adsorption of Cu (II) on nanoscale magnetite in aqueous solutions. Desalination 2011;276(1):154-60.
18. Alpat SK, Ozbayrak O, Alpat S, Akcay H. The adsorption kinetics and removal of cationic dye, Toluidine Blue O, from aqueous solution with Turkish zeolite. J Hazard Mater 2008; 151:213–20.
19. Brunauer S, Emmett PH, Teller E. Adsorption of Gases in Multimolecular Layers. J Am Chem Soc 1938; 60:309–19.
20. Khosravi M, Azizian S. Adsorption of anionic dyes from aqueous solution by iron oxide nanospheres. J Ind Eng Chem 2014; 20:2561–7.
21. Silva M, Oliveira M, Avelino M, Fonseca M, Almeida R, Filho E. Adsorption of an industrial anionic dye by modified-KSF-montmorillonite: Evaluation of the kinetic, thermodynamic and equilibrium data. Chem Eng J 2012; 203:259–68.
22. Zhang YR, Wang SQ, Shen SL, Zhao BX. A novel water treatment magnetic nanomaterial for removal of anionic and cationic dyes under severe condition. Chem Eng J 2013;233:258–64.
23. Azizian S. Kinetic models of sorption: a theoretical analysis. J Colloid Interface Sci 2004; 276:47–52.
24. Langmuir I. The adsorption of gases on plane surfaces of glass, mica and Platinum. J Am Chem Soc 1918; 40:1361–1403.
25. Freundlich H, Heller W The adsorption of cis- and trans-Azobenzene. J Am Chem Soc 1939; 61:2228–30.